# Empirical Modeling and Optimization of Pressure Coupled Infusion Gyration Parameters for the Nanofiber Fabrication

Xianze Hong[§], Anthony Harker[†], Mohan Edirisinghe*

§Department of Mechanical Engineering,

University College London (UCL), Torrington Place, London WC1E 7JE, UK

†Department of Physics and Astronomy,

University College London (UCL), Gower Street, London WC1E 6BT, UK

*Department of Mechanical Engineering,

University College London (UCL), Torrington Place, London WC1E 7JE, UK

E-mail: m.edirisinghe@ucl.ac.uk

## Abstract

Pressure coupled infusion gyration (PCIG) is a novel promising technique for economical and effective mass production of nanofibers with desirable geometrical characteristics. The average diameter of spun fibers significantly influences the structural, mechanical and physical properties of the produced fiber mats. Having a comprehensive understanding of the significant effects of PCIG experimental variables on the spun fibers is beneficial. In this work, response surface methodology (RSM) was utilized to explore the interaction effects and the optimal PCIG experimental variables for achieving the desired morphological characterization of fibers. The effect of experimental variables, namely solution concentration, infusion (flow) rate, applied pressure and rotational speed, was studied on the average fiber diameter and standard deviations. A numerical model for the interactional influences of experimental variables was developed and optimized with a non-linear interior point method that can be utilized as a framework for selecting the optimal conditions to obtain poly-ethylene oxide (PEO) fibers with desired morphology (targeted average diameter and narrow standard deviation). The adequacy of the models was verified by a set of validation experiments. The results proved that the predicted optimal conditions were able to achieve the average diameter that matched the pre-set desired value with less than 10% of difference.

Key-words: Pressure coupled infusion gyration, nanofiber, modeling, response surface methodology, process optimization

## 1. Introduction

Due to the unparalleled ability to make complicated and customized geometric shapes directly from various materials, the demand for additive manufacturing technology is increasing [1-6]. Nanofibers, a one-dimensional nanomaterial with versatile properties and complex structures, can be randomly or directionally arranged in continuous fiber mats or bundles that have ordered internal morphology, such as porous, core sheaths or hollow fibers, and multi-channel microtubules [7-9]. Ultrafine fibers garnered much attention due to their various outstanding characteristics, such as high surface to volume ratio, high porosity, and excellent mechanical properties [7][8-14]. Despite their versatility, the use of nanofibers is still limited by the lack of proper mass production methods [11].

Electrospinning is a versatile and promising technique using electrostatic forces to fabricate ultrafine fibers. However, the utilization of electrospinning is highly restricted by several drawbacks that severely affect its yield and production quality, including sensitivity to the stability of spinning jet and conductivity of polymer solutions, random orientations of fabricated fibers, high cost due to required high voltage, low production rate and the larger nozzle sizes that are required due to the high viscosity of the biopolymers used [15,16]. Although increasing the number of needles [17] and collecting fibers by a rotating drum [18] can improve its production rate and orientations, these will introduce secondary effects, for instance, a capillary effect, and therefore further increased cost. Pressure coupled infusion gyration (PCIG) is a novel method, based on centrifugal rotation mainly derived from industrial jet spinning, which can overcome the above limitations of electrospinning. The experimental studies of PCIG in our previous work [14] showed that this method is able to produce finer fibers at sub-micron or micrometer level with fewer restrictions on material properties than electrospinning. The method also overcomes the discontinuous production of other rotation based processes, for instance, force spinning [19]. PCIG affords new advanced features beyond bulk materials and it can economically and consistently produce uniaxially aligned 3D fiber bundles [14].

Determination of optimum levels of operational variables in experiments by conventional methods is often carried out by a one-variable-at-a-time technique, just monitoring the effect of one variable on the experimental responses, fixing others at a constant level. The main drawbacks of this method are neglect of the interaction effects between different variables, as the interaction effect sometimes could be more critical in the process e.g. synergism, antagonist etc, so the full impacts of variables on the response cannot be studied [20]. Additionally, this method is highly time and cost-consuming, yet does not guarantee the determination of optimal conditions among the variable sets. In order to overcome these disadvantages of the traditional optimization method, multivariate statistical techniques can be applied to optimize the experimental process, and response surface methodology (RSM) is the most popular one. RSM is a collection of mathematical and statistical techniques for empirical model development and

optimizing based on the experimental data. RSM has important application in determining the behavior of data sets for statistical forecasting. It can define the influence of independent variables individually or in combination on a response or a set of responses of a process, and simultaneously optimize the levels of experimental variables to attain the optimal performance of the system. Some examples of the RSM applications of optimization of chemical or biomedical process are enzymatic processing [21,22], heat transfer with nano-fluid [23,24], micro-extraction for pre-concentration [25], ultrasonicated adsorption and extraction process [26-28], cooling strategy for Li-ion batteries [29] and fiber manufacturing [30-33]. RSM is used to approximate the functional relationship between the independent variables and the process response based on experimental data, and it is valuable in obtaining insight of variable contributions through the coefficients in the developed model. The developed model can be saved and used as a prediction tool for the optimal combinations of experimental variables that can achieve the optimum response. Moreover, RSM is scalable to design and predict a model equation with a higher degree than the second order, but it should be noted that the selection of the order should be conducted after carefully analyzing the input data. A lower order model may not be able to capture the variance of the data and result in a highly biased model (also known as underfitting), and a higher order may lead the fitting curve pass through most of the data points and result in a less generalized mode (also known as overfitting). RSM should not be extrapolated outside the range that contains the original observations, and the developed model may not explicitly express the physical meaning of the system or process under investigation.

In the present work, PEO was used as a model material, which is a water-soluble polymer. We investigated the empirical modeling and optimizing of PEO fibers produced by the PCIG process. In the fitting procedure, we considered a physical frame of rotary jet spinning to have a better understanding of the physical meaning in the spinning process [34]: this part of the work was detailed in our previous work [35]. Optimization of PCIG spinning process was performed to attain combinations of experimental variables that were able to achieve a targeted average fiber diameter with a narrow standard deviation of diameter. The experimental variables studied in the present work are solution concentration, applied pressure, rotational speed and infusion flow rate. In the last step, to verify the applicability and reproducibility of the developed model, a set of experiments was carried out at the predicted optimal conditions, and their results compared with our targeted value. The potential of PCIG with more volatile solvents was not fully explored. Early indications are that due to evaporation it might not be as promising as with water-based solvents.

## 2. Materials and methods

### 2.1. Materials

In this work, Poly-(ethylene oxide) (PEO, molecular weight (Mw): $2 \times 10^5$ g $mol^{-1}$) was the selected polymer, which was purchased from Sigma Aldrich, and deionized water was used as the solvent.

### 2.2. Experiments

PCIG apparatus (see **Figure 1**) used in this work consists of a cylindrical pot 40 mm in height and 60 mm in diameter. The rotational pot was equipped with 20 orifices placed equidistantly (9 mm) and located on the wall of the vessel at the same height, and each ≈ 0.5 mm in diameter. Nanofiber's geometry and cross-section can be customized by the geometry and size of vessel and orifices [36]. The rotational pot was driven by a motor, which could provide various rotating speeds up to 36000 rpm. A nitrogen cylinder was used to provide applied pressure (up to $3 \times 10^5$ Pa). A syringe pump (PHD Ultra 4400, Harvard Apparatus Ltd., Edenbridge, UK) connected at the bottom of the pot by a plastic tube was used to control polymer solution flow (up to 5000 µL $min^{-1}$) and continuously feeds into the pot during processing. A stationary copper mesh was placed around the pot (100 mm) for convenient collection of fibers and the distances between the vertical wires are 25 mm. We have used 100 mm based on optimization in our previous work [14,35]. During experiments, the ambient environment parameters including humidity (38.5%) and temperature (25 °C) were fixed. PCIG effectively uses induced pressure and high-speed rotation of the pot to force polymer jets to emerge from orifices parallelly to create fiber fabrications. The spun fibers were assessed using a field emission scanning electron microscope (JSM-6301F), and the fiber diameters were determined from random fibers at different locations of each sample using Image J software.

In this work, nanofibers were prepared by changing four variables: solution's concentration, pressure, rotational speed and infusion (flow) rate. The experiments were conducted at different levels of each parameter: four levels of concentration(c) (5, 10, 15, 21 wt%), three levels of applied pressures(p) (0.1, 0.2, 0.3 MPa), three levels of rotational speeds(g) (12000, 24000, 36000 rpm) and six levels of flow rate(f) (500, 1000, 2000, 3000, 4000, and 5000 µL $min^{-1}$).

**Figure 1 Pressure coupled infusion gyration set-up (a) and fiber formation process captured using a high speed camera (b)**

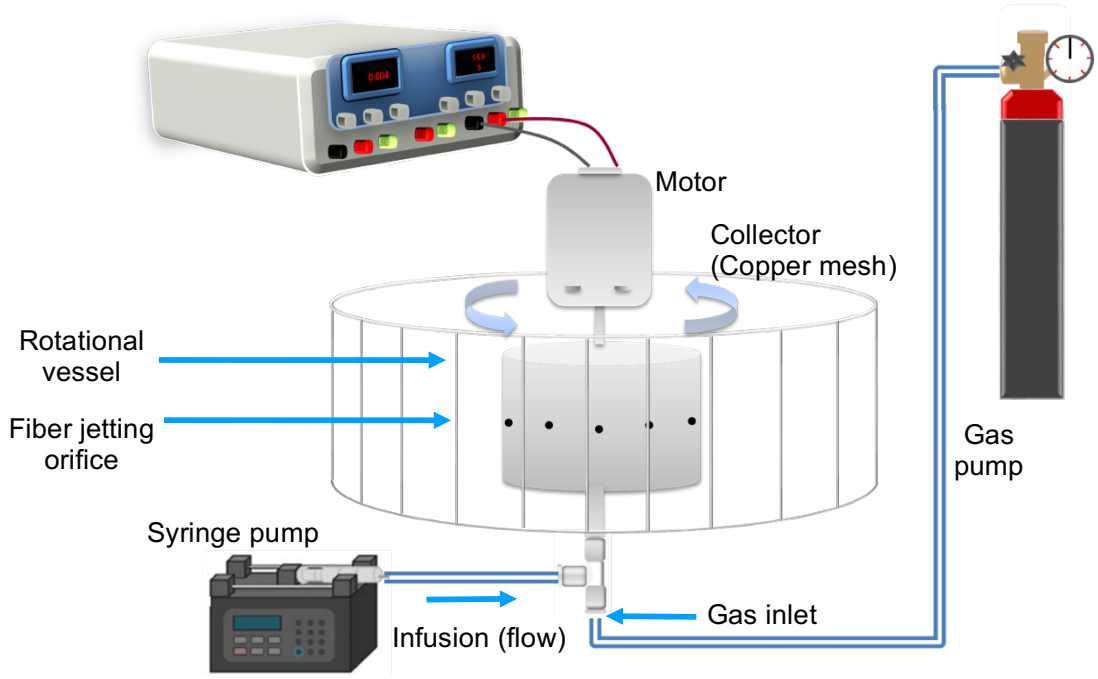


(a)

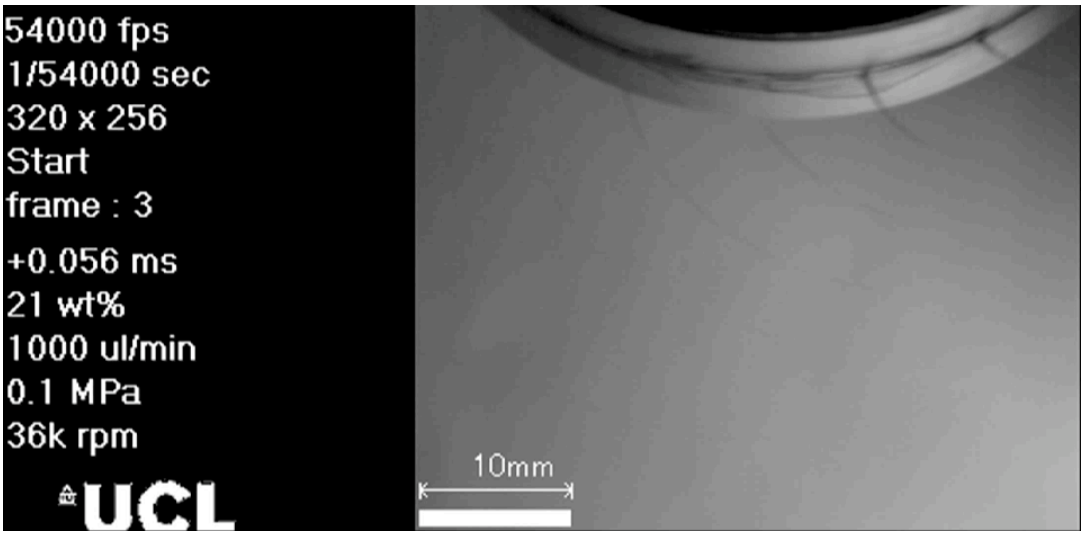


(b)

## 2.3. Modeling

RSM was applied with four variables (solution concentration, pressure, rotational speed and infusion flow rate) to determine the influences of the experimental parameters in the spinning process and the optimal conditions to obtain the desired diameters. In this study, in order to investigate the effects of all the control variables, we carried out 120 experiments with different combinations of experimental variables established at different levels. For the observation of each experiment, more than 100 fiber diameters were obtained from the random fibers of each sample, and each value of mean diameter was used as

one input entry in the model fitting procedure, except the 19 combinations which gave beads or beaded fibers, and these were excluded from the modeling.

The mean fiber diameter was considered as the response of the PCIG system and Mathematica was used to process the experimental results using a least squares algorithm. In order to achieve a significant regression, most of the variation in the experimental results were explained by the response function, and the rest were dealt by the residuals in fitting. For each response function, the analysis of variance (ANOVA) was conducted to assess the source of experimental variance and evaluate the regression significance. In addition, the adequacy of the models that fit experimental data was compared using the Akaike information criterion (AIC) and Adjusted $R^2$. The Akaike Information Criterion (AIC), a model selection criterion established on the basis of information entropy, can be calculated by applying maximum likelihood theory and increases its value to penalize the redundant variables in the model. A relative higher value is unfavorable for a fitted model as then higher residuals exist between the fitting and experimental results. Three-dimensional graphical representations of the system output were used to explore the interaction effects of the variables on the diameter.

## 3. Results and discussion

### 3.1. Analysis of response surface

PCIG experimental variables (flow rate, concentration, pressure and rotational speed) affect the fiber diameter in different extents. Their effects on PEO average fiber diameter are demonstrated in **Figure 2**.

**Figure 2 Response surface plots showing effect on fiber diameters as a function of: (a) flow rate and concentration, (b) concentration and pressure, (c) concentration and rotational speed, (d) flow rate and rotational speed**

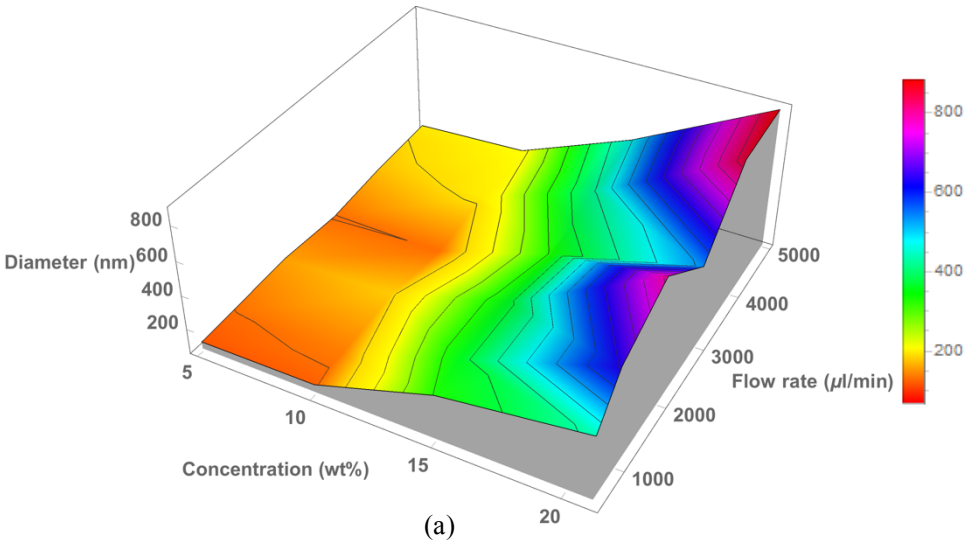


(a)

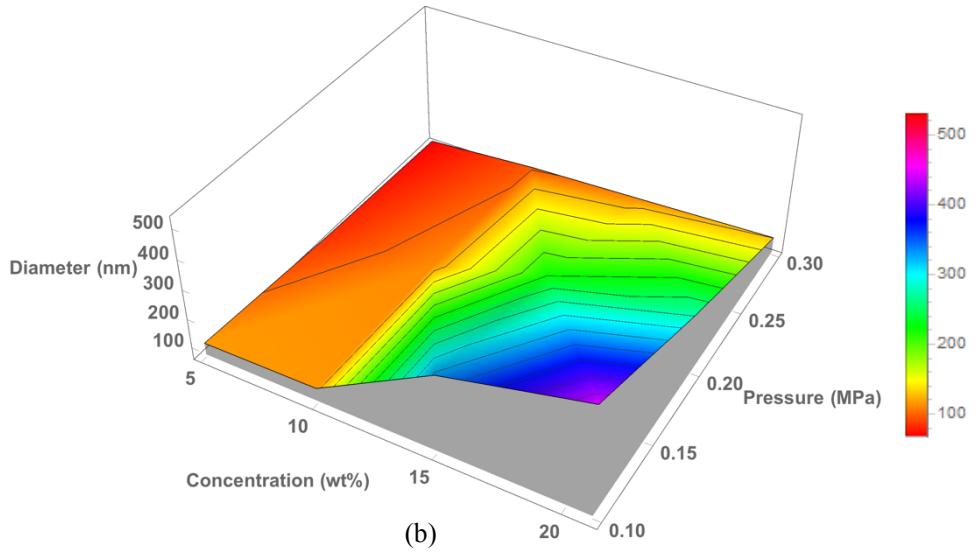
Diameter (nm)
500
400
300
200
100
5
10
15
20
Concentration (wt%)
0.10
0.15
0.20
0.25
0.30
Pressure (MPa)
500
400
300
200
100

(b)

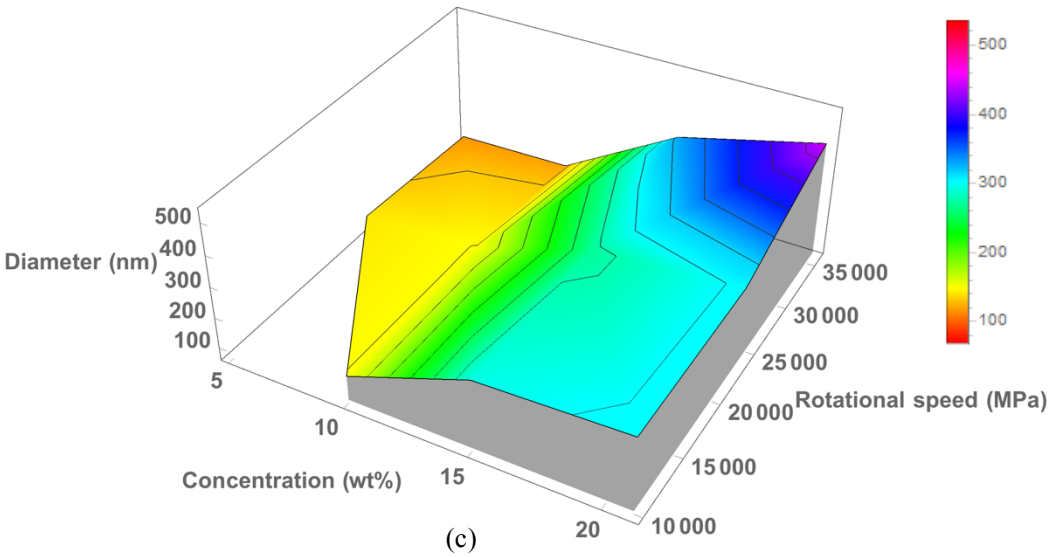
Diameter (nm)
500
400
300
200
100
5
10
15
20
Concentration (wt%)
10 000
15 000
20 000
25 000
30 000
35 000
Rotational speed (MPa)
500
400
300
200
100

(c)

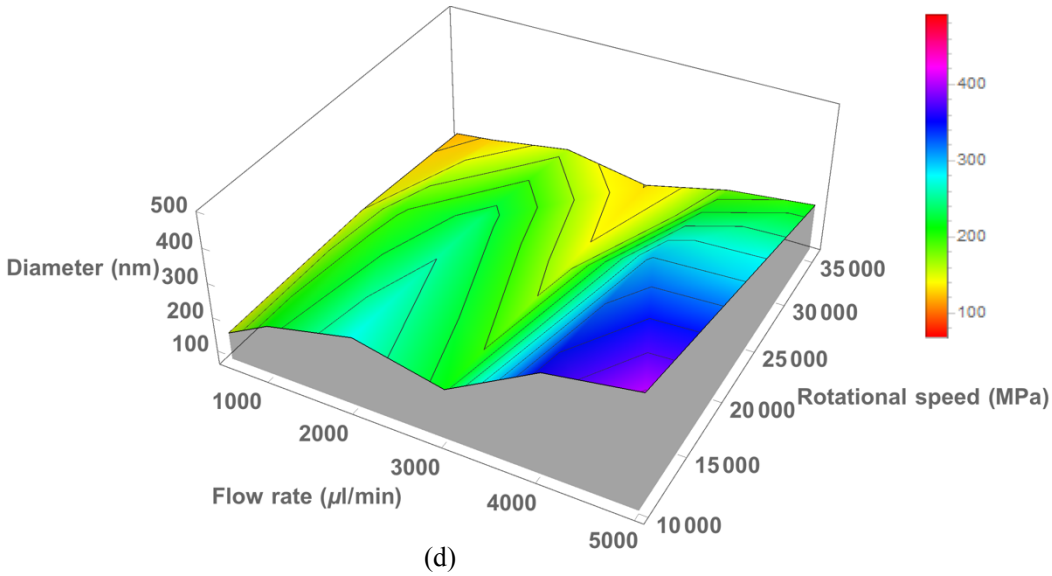
Diameter (nm)
500
400
300
200
100
1000
2000
3000
4000
5000
Flow rate (μl/min)
10 000
15 000
20 000
25 000
30 000
35 000
Rotational speed (MPa)
400
300
200
100

(d)

During spinning, there is a hydrostatic pressure at the orifices, which is constant when the processing variables are fixed and it will be enhanced by the increasing of flow rate. However, the hydrostatic force is much smaller than the governing centrifugal effect. Hence, the fiber formation process could be simply seen as a balance between the surface tension of polymer solutions and external forces (gravitational force and centrifugal force). At the start of spinning, a steady and continuous polymer solution flow is injected from the bottom of the rotational vessel. Then, the polymer solution emerges from the orifice to form the droplet, and there is a Marangoni effect that occurs due to the surface tension gradient across the liquid-air interface of the droplet. This causes the solution to pass to the tip of the droplet to form a polymer jet. This jet is further stretched by the pressure difference in the two sides of the orifice and the centrifugal effect. Finally, the ejected jet thins and solidifies to form fiber as solvent evaporation takes place.

A trend of reduction in the fiber diameter with increasing the pressure and rotational speed is observed. The solution blowing combines with centrifugal force that acts against the surface tension of the solution, thus enabling the generation of fibers from the pot orifices. A high speed of rotation enhances the deformation of the solution by increasing the centrifugal effect. Enhanced gas blowing induced by high pressure would reinforce the thinning effect and also promotes solvent evaporation that takes place along the radial direction of spinning. However, the increased gas blowing would also enhance the jet's instability at the orifices, which may promote formation of the beads or beaded fiber.

The impact of polymer concentration on the formation and morphology of the fabricated fiber by tuning solution's fluid properties, for example, the viscosity and degree of chain entanglement, is of crucial importance for uniform fiber formation [37,38]. The critical polymer concentration of chain entanglement can be estimated using the intrinsic viscosity of the PEO solution and its estimation by Barnes et al's method [39] and is ≈ 0.7 wt%. In the fiber generation process, a higher concentration would hinder fiber-extension and stabilize the polymer jet, due to the greater resistance of the solution to stretching by the combined effects (of gas blowing and centrifugal force) on the jet, hence promoting thicker fiber at all conditions. As can be seen in **Figure 1S** (see supplementary material [35]), there was a steeper slope in changes of average fiber diameter with concentration and pressure level, which implied the response was more sensitive to concentration and pressure than flow rate and rotational speed.

The flow rate regulates volume and mass of polymer solution transferring through the orifices. Thompson et al [16] used a regression analysis to prove that a jet initially with a larger diameter will lead to a larger final jet diameter. A higher flow rate would allow less time for fiber stretching and solvent evaporation, hence promoting thicker fiber during spinning, which was observed in our previous work [14]. However,

in some cases, the increases of flow rate actually do not lead to the increases of average fiber diameter. We observed the average fiber diameter was increasing first then dropped at 3000 μL $min^{-1}$, and subsequently increased when increasing the flow rate further. The same phenomenon also occurred in the electrospinning studies by Schoenmaker et al, [40] Faridi-Majidi et al [41] and Adabi et al [42]. It suggests that the reduction in average fiber diameter is due to a balance of volume of solution transfer through the orifice operating in competition with other experimental variables including flow rate and pressure. Moreover, the generation of multiple secondary jets from the initial jet may also contribute to this phenomenon, as the solidified polymer solution at orifice forces the jet eruption from the ambient unsolidified surface, which results in smaller diameter formed by secondary jets compared to an initial jet.

### 3.2. Model fitting

The optimum experimental conditions were defined as the combinations of processing parameters that can afford the prepared fibers with our desired fiber diameters and small standard deviations. The stages that explore the optimum conditions are model fitting, variable optimization, and experimental validation. In our previous study, [35] we discussed the fitting process in detail, both linear and nonlinear formats, as we assumed that linear or nonlinear mapping might exist between the four variables and fiber diameters. In the fitting procedure, we developed functions for the response by exploring fitting to multivariate experimental results according to the trends of variation of response displayed in **Figure 2** and **Figure 1S** (see supplementary material [35]), including: a quartic relationship between flow rate and diameter; quadratic relationships are to other variables; inverse dependences between pressure/rotational speed and diameter.

The nonlinear response function that we fitted using the non-linear method based on the Levenberg-Marquardt algorithm is as determined in **Eq. 1**[*]. The resulting Adjusted $R^2$ was 95.7% and an AIC value was achieved at 1128. As the Adjusted $R^2$ represents the total variability level that can be expected from the fitted model, this result indicated the nonlinear model is sufficient to explain the relationship between variables, and it probably can be used for prediction of the desired diameter.

$$f_d(c,p,f,g) = \left(1818.47\,f - 1.20\,f^2 + (3.04\times10^{-4})\,f^3 - (2.56\times10^{-8})\,f^4\right)\left(1 + 0.12\,c + (9.26\times10^{-3})\,c^2\right)\,e^{0.14/p}\,\left(1/g - 7046.28/(g)^2\right) \quad (1)$$

[*] Variables in equations (1) and (2) are: c: polymer concentration; p: applied pressure; f: infusion flow rate; g: rotational speed.

For exploring the statistical characteristics of the standard deviation of average diameter, regression analysis was also performed for standard deviation. We found that there was a strong linear correlation existing between the fiber diameter and standard deviation in our experimental results. For the optimization purpose of obtaining a narrow standard deviation, we predicted the standard deviations based on the mean fiber diameters that used as the input, and computed the differences between the predicted value and the experimental value of the standard deviations. The fitted linear-quadratic function for the difference of standard deviation of average diameter is shown in **Eq.2**, where $f_s$ is the standard deviation difference of fiber diameter. **Eq.2** gave an AIC value of 924 and Adjusted $R^2$ of 80% and its ANOVA results are listed in **Table 1**. The significance of each factor was determined by considering a 5% confidence level of P-value and in our previous work [35] we found that the concentration had the most important impact on the mean fiber diameter. The estimated coefficients of the fitted linear model are as presented in **Table 1**, where the SS is the sum of squared observation deviations. The ANOVA table showed that the fitted model was hierarchically well formulated, in other words, it had included the major effects presented in the high order terms. For instance, the pressure observed the highest relative impact on the standard deviation differences. The term in concentration and flow rate were the subdominant factors. There was not enough statistical evidence to justify the interaction term of flow rate/pressure (fp). Even if the term was not significant, their individual values had significant effects on diameter. Hence, the interaction term should also be incorporated into the model, as well as for the quadratic term of concentration.

$$f_s(c, p, f, g) = \alpha_0 - \alpha_1 c + \alpha_2 c^2 + \alpha_3 f - \alpha_4 cf - \alpha_5 c/g + \alpha_6 /g^2 - \alpha_7 /p + \alpha_8 c/p - \alpha_9 f/p + \alpha_{10} /p^2 \quad (2)$$

**Table 1. ANOVA table of the fitted model of standard deviation reference to Eq. 2**

| | Estimated coefficient ($\alpha_n$) | SS | F-statistics | P-Value |
|---|---|---|---|---|
| 1 | 94.53 | | | |
| c | 7.26 | 2813.95 | 5.75 | 0.02 |
| $c^2$ | 0.14 | 115.27 | 0.24 | 0.63 |
| f | 0.02 | 2293.26 | 4.69 | 0.03 |
| cf | $9.58\times10^{-4}$ | 4134.27 | 8.45 | $4.59\times10^{-3}$ |
| cg | 52951.70 | $2.00\times10^{4}$ | 40.90 | $7.00\times10^{-9}$ |
| $g^2$ | $5.31\times10^{9}$ | 4988.81 | 10.20 | $1.93\times10^{-3}$ |
| p | 34.99 | $4.81\times10^{4}$ | 98.40 | $4.20\times10^{-16}$ |
| cp | 1.55 | $4.23\times10^{4}$ | 86.48 | $8.20\times10^{-15}$ |
| fp | $1.12\times10^{-3}$ | 1368.65 | 2.80 | 0.10 |

| | | | | |
|---|---|---|---|---|
| $p^2$ | 1.91 | 4294.58 | 8.78 | $3.89\times10^{-3}$ |

### 3.3. Process variables optimization

The goal of optimization was to find the most suitable experimental conditions for fabricating nanofibers with a desirable diameter, and in this paper, we used 300 nm as an example. The effect of the relationship between experimental variables on diameter is illustrated using three dimensional graphs. The data were generated by first pre-setting a targeted diameter and keeping three variables within a respective intermediate range at a time and varying the fourth to achieve the targeted diameter. The distribution of allowable experimental variables which we predicted would lead to the targeted diameter can be seen in **Figure 3**. The color for each dot in the graphs stands for the level of the changing variable, so colors from violet to red, correspond to changing the variable's value increases from low to high. From **Figure 3 (a)** and **(b)**, a clear linear boundary was defined between concentration and pressure, and the correlation matrix of the operational variables (**Figure 4**) showed that there was a strong positive correlation between concentration and pressure, and a weak positive correlation existed between flow rate and rotational speed. Physically, this means that if the concentration of the polymer solution was increased it became more viscous, so higher pressure was needed to get solution out through the orifices of rotational pot, but also that a decrease in the flow rate should be accommodated to allow more time for the centrifuge effect to stretch the jetting fibers and increase the gyration speed to enhance the centrifugal effect.

**Figure 3 3D plots of experimental variables modeled with non-linear model (Eq.1) for pre-defined (targeted) 300 nm average diameter.**

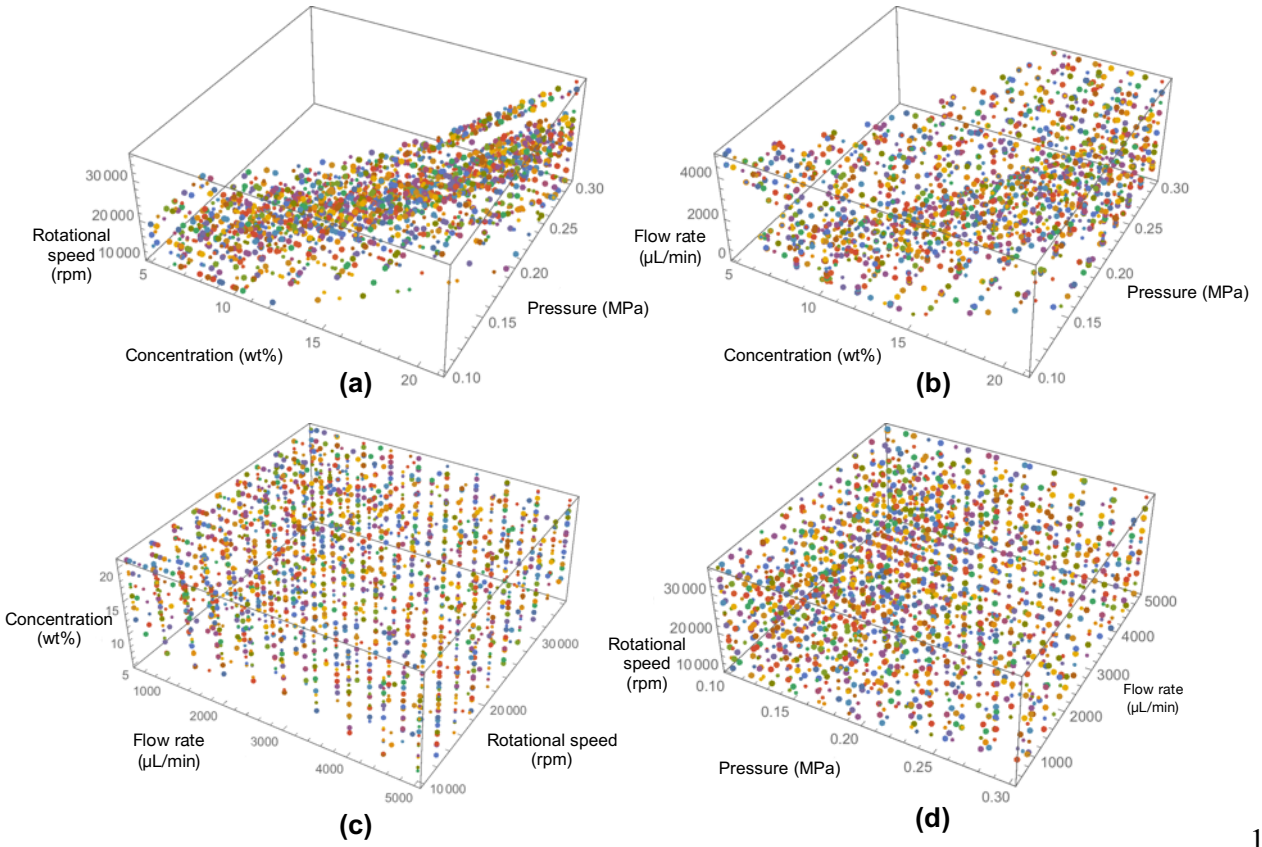

**Figure 4 Correlation matrix of experimental variables**

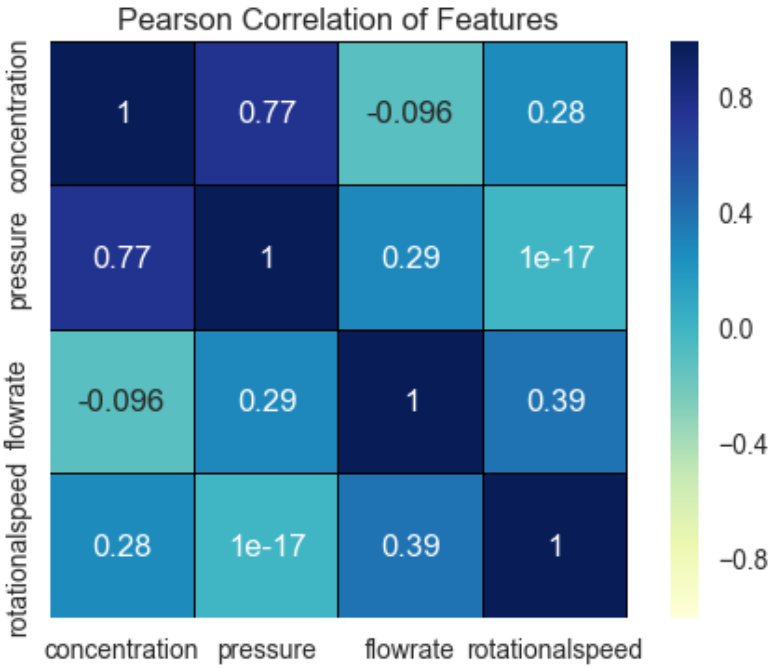


From the optimization point of view, the term of "desirability" was defined as that involved two responses from numerical optimization in this study, the final response should explore the points that maximized the function of "desirability" [20]. Numerical optimization utilized the model that developed in section 3.2 to search the design space, to obtain groups of variables that generate the defined targeted nanofibers based on minimizing the cost function value (maximizing the desirability). A suitable cost function for achieving the "desirable" diameter with narrow spread is given by **Eq.3**.

$$f_e(d_0, w_1, w_2, c, p, f, g) = w_1(d_0 - f_d(c,p,f,g))^2 + w_2\,(f_s(c,p,f,g)\,|f_s(c,p,f,g)|) \quad (3)$$

where $d_0$ is the targeted diameter (in nm), $w_1$ and $w_2$ were the weighted factors of diameter part and standard deviation part of the cost function and both were initialized as one at the start of the optimization process. As the PCIG is a robust process for mass production of nanofibers, and the rotational speed showed a weaker effect in the regression analysis, it was not necessary to be tuned to very high precision. Hence, in the process of optimization, we selectively confined the ranges of the experimental variables to those which were reasonable for the real experiments, including concentrations (5 - 20 wt%), pressure (0.1 - 0.3 MPa), flow rate (500-5000 μL $min^{-1}$), rotational speed (12000 - 36000 rpm). We compared the results of several optimization algorithms (direct search method and gradient-based method), and non-linear interior point algorithm offered better results. Finding global optimums can be arbitrarily difficult even without constraints, so the methods used may fail. It may often be useful to optimize the function multiple times and pick the best results (global optimum or fine local optimum) [43]. Six groups of experimental variables were generated, as indicated in **Table 2**. Interestingly, there were

recommendations for high concentrations (over 10 wt%) for all of the optimal (including comparative local and global optimum) conditions and most of them were higher or equal to 15 wt%. This result is in agreement with other studies which conclude that the optimal experimental conditions for the spun fiber diameter were highly dependent on the polymer concentration, [44,45] and it is suggested that the diluted polymer solution (e.g. 5 wt%) may lead to the wider spread of fiber diameter. The range of produced mean diameter in our experiments was around 50 – 850 nm, so this model is best suited to be used for the prediction of the set of parameters that can give the fiber diameter within this range. Additionally, the only variable characteristic of fluid properties is polymer concentration in this model. If it warrants to be used for different polymer and solvent combinations, the model should be revised to include physical properties, such as viscosity and surface tension would have to be developed.

### 3.4. Validation of the model

Up to this stage of our study, we computationally optimized the PCIG parameters of polymer concentration, pressure, flow rate and rotational speed to achieve nanofibers with targeted average diameter with a narrow spread of diameters. In order to check the reliability of the RSM models, a set of experiments was conducted at the optimal conditions and these results are described below.

**Table 2. Validation results of the predicted optimal conditions**

| Conditions No. | Concentration (wt%) | Rotational speed (rpm) | Pressure (MPa) | Flowrate (μL $min^{-1}$) | Predicted diameter (nm) | Validated diameter (nm) |
|---|---|---|---|---|---|---|
| 1 | 11 | 12000 | 0.1 | 566 | 316.58 | 348 |
| 2 | 15 | 12000 | 0.2 | 1021 | 298.59 | 271 |
| 3 | 15 | 24000 | 0.2 | 3323 | 299.83 | 297 |
| 4 | 20 | 24000 | 0.2 | 685 | 299.88 | 291 |
| 5 | 20 | 36000 | 0.2 | 1553 | 298.56 | 297 |
| 6 | 20 | 36000 | 0.3 | 4983 | 289.59 | 295 |

**Figure 5 Scanning Electron micrographs of PEO fibers generated for validation experiments set in Table 2 at conditions: (a):1, (b):2, (c):3, (d):4, (e):5, (f):6.**

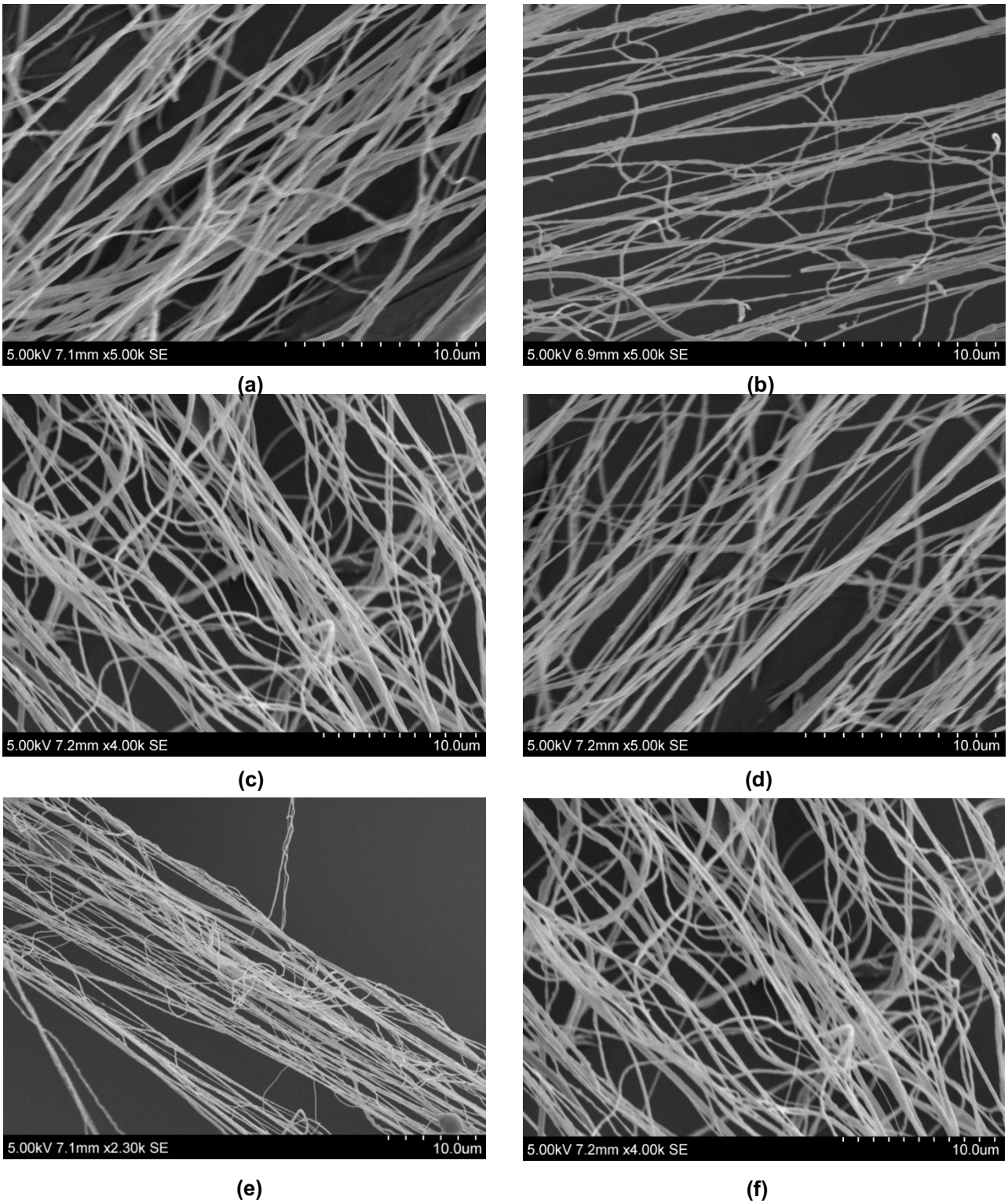


The produced fibers were collected at the 100 mm collection distance (from orifices to collector), and the corresponding images of PEO nanofibers in the optimal conditions were acquired by SEM (Figure 5). The results of validation experiments derived from the observations in Figure 5 are shown in Table

2, which depicted the measured fiber diameters were in good agreement with the values that are predicted using the optimized model. This suggests that the proposed model is able to predict the operational conditions for fiber diameter with high accuracy.

## 4. Conclusions

The present study focuses on understanding how the PCIG experimental variables, namely solution's concentration, pressure, flow rate and rotational speed, affected the morphological features of spun PEO nanofibers. Response surface methodology was utilized to optimize the experimental variables for fabricating PEO fibers with a desired diameter and narrow standard deviation. A non-linear model that was fitted with a quartic equation and another linear model that was fitted with a quadratic equation was developed for the prediction and optimization of average fiber diameter and standard deviation of diameter, respectively. These two models were optimized by omitting the non-significant variables. The resulting Adjust $R^2$ and AIC values indicated that there was no evidence of lack of fit. The results of ANOVA demonstrated that the standard deviation differences of diameter had experienced the highest impact from the pressure and the average diameter was strongly affected by the concentration, and besides, the flow rate and rotational speed played subdominant roles for controlling the spun fiber morphologies. The optimal conditions of experiments were found by developing a cost function that uses the fitted models and optimizing it with non-linear interior point methods. Interestingly, for obtaining the desired diameter with narrow standard deviation, a condition with higher concentration and moderate pressure was suggested. Validation experiments verified the adequacy (accuracy) of our models. PEO nanofibers (close to averagely 300 nm diameter in this study) were obtained at the optimal conditions given in **Table 2**. The difference between predicted and validated results (experimentally observed) was less than 10%. It can be concluded that the proposed models are in good agreement with the validation results, the models were applicable and replicable in determining the optimal experimental variables for getting the desired PEO nanofibers with the intended diameter. However, it should be noted that the effects of rheology of different types of polymer solutions were not included in this study, this does not impact PEO-water solutions but could affect other non-aqueous polymer solution.

## Acknowledgements

The authors thank the Engineering and Physical Sciences Research Council (EPSRC), UK for providing the financial support for the exploitation of pressurised gyration research (EP/L 023059/1 and EP/N 034228/1) at UCL. Data supporting this study are provided in the paper and in supplementary information.

## Author information

Xianze Hong: xianze.hong.13@ucl.ac.uk

Anthony Harker: a.harker@ucl.ac.uk

Mohan Edirisinghe: m.edirisinghe@ucl.ac.uk

## References

[1] Khani, N., Nadernezhad, A., Bartolo, P., & Koc, B. (2017). Hierarchical and spatial modeling and bio-additive manufacturing of multi-material constructs. *CIRP Annals*, *66*, 229-232.

[2] Mota, C., Puppi, D., Chiellini, F., & Chiellini, E. (2015). Additive manufacturing techniques for the production of tissue engineering constructs. *Journal of tissue engineering and regenerative medicine*, *9*, 174-190.

[3] Nadernezhad, A., Khani, N., Skvortsov, G. A., Toprakhisar, B., Bakirci, E., Menceloglu, Y., Unal, S., & Koc, B. (2016). Multifunctional 3D printing of heterogeneous hydrogel structures. *Scientific reports*, *6*, 33178.

[4] Ning, F., Cong, W., Hu, Y., & Wang, H. (2017). Additive manufacturing of carbon fiber-reinforced plastic composites using fused deposition modeling: Effects of process parameters on tensile properties. *Journal of Composite Materials*, *51*, 451-462.

[5] Ning, F., Cong, W., Qiu, J., Wei, J., & Wang, S. (2015). Additive manufacturing of carbon fiber reinforced thermoplastic composites using fused deposition modeling. *Composites Part B: Engineering*, *80*, 369-378.

[6] Bhushan, B., & Caspers, M. (2017). An overview of additive manufacturing (3D printing) for microfabrication. *Microsystem Technologies*, *23*, 1117-1124.

[7] Torres-Giner, S., Pérez-Masiá, R., & Lagaron, J. M. (2016). A review on electrospun polymer nanostructures as advanced bioactive platforms. *Polymer Engineering & Science*, *56*, 500-527.

[8] Zheng, J., Zhang, H., Zhao, Z., & Han, C. C. (2012). Construction of hierarchical structures by electrospinning or electrospraying. *Polymer*, *53*, 546-554.

[9] Li, Z., & Wang, C., One-dimensional nanostructures: electrospinning technique and unique nanofibers, Springer, 2013.

[10] Hong, X., Edirisinghe, M., & Mahalingam, S. (2016). Beads, beaded-fibres and fibres: Tailoring the morphology of poly (caprolactone) using pressurised gyration. *Materials Science and Engineering: C*, *69*, 1373-1382.

[11] Parhizkar, M., Mahalingam, S., Homer-Vanniasinkam, S., & Edirisinghe, M. (2018), Latest developments in innovative manufacturing to combine nanotechnology with healthcare, *Nanomedicine*, *13, 5-8*.

[12] Brako, F., Luo, C., Craig, D. Q., & Edirisinghe, M. (2018). An Inexpensive, Portable Device for Point-of-Need Generation of Silver-Nanoparticle Doped Cellulose Acetate Nanofibers for Advanced Wound Dressing. *Macromolecular Materials and Engineering*, *303*, 1700586.

[13] Altun, E., Aydogdu, M. O., Koc, F., Crabbe-Mann, M., Brako, F., Kaur-Matharu, R., Ozen, G., Kuruca, S. E., Edirisinghe, U., & Gunduz, O., & Edirisinghe, M. (2018). Novel Making of Bacterial Cellulose Blended Polymeric Fiber Bandages. *Macromolecular Materials and Engineering*, *303*, 1700607.

[14] Hong, X., Mahalingam, S., & Edirisinghe, M. (2017). Simultaneous Application of Pressure-Infusion-Gyration to Generate Polymeric Nanofibers. *Macromolecular Materials and Engineering*, *302*, 1600564.

[15] Forward, K. M., & Rutledge, G. C. (2012). Free surface electrospinning from a wire electrode. *Chemical Engineering Journal*, *183*, 492-503.

[16] Thompson, C., Chase, G. G., Yarin, A., & Reneker, D. (2007). Effects of parameters on nanofiber diameter determined from electrospinning model. *Polymer*, *48*, 6913-6922.

[17] Zhou, F. L., Gong, R. H., & Porat, I. (2009). Mass production of nanofibre assemblies by electrostatic spinning. *Polymer International*, *58*, 331-342.

[18] Doergens, A., Roether, J. A., Dippold, D., Boccaccini, A. R., & Schubert, D. W. (2015). Identifying key processing parameters for the electrospinning of aligned polymer nanofibers. *Materials Letters*, *140*, 99-102.
[19] Hammami, M. A., Krifa, M., & Harzallah, O. (2014). Centrifugal force spinning of PA6 nanofibers–processability and morphology of solution-spun fibers. *the Journal of the Textile Institute*, *105*, 637-647.
[20] Bezerra, M. A., Santelli, R. E., Oliveira, E. P., Villar, L. S., & Escaleira, L. A. (2008). Response surface methodology (RSM) as a tool for optimization in analytical chemistry. *Talanta*, *76*, 965-977.
[21] Nongonierma, A. B., Maux, S. L., Esteveny, C., & Fitzgerald, R. J. (2017). Response surface methodology applied to the generation of casein hydrolysates with antioxidant and dipeptidyl peptidase IV inhibitory properties. *Journal of the Science of Food and Agriculture*, *97*, 1093-1101.
[22] Ashrafi, S., Nasseri, S., Alimohammadi, M., Mahvi, A., & Faramarzi, M. (2016). Optimization of the enzymatic elimination of flumequine by laccase-mediated system using response surface methodology. *Desalination and Water Treatment*, *57*, 14478-14487.
[23] Shirvan, K. M., Mamourian, M., Mirzakhanlari, S., & Ellahi, R. (2017). Numerical investigation of heat exchanger effectiveness in a double pipe heat exchanger filled with nanofluid: A sensitivity analysis by response surface methodology. *Powder Technology*, *313*, 99-111.
[24] Iranmanesh, S., Mehrali, M., Sadeghinezhad, E., Ang, B. C., Ong, H. C., & Esmaeilzadeh, A. (2016). Evaluation of viscosity and thermal conductivity of graphene nanoplatelets nanofluids through a combined experimental–statistical approach using respond surface methodology method. *International Communications in Heat and Mass Transfer*, *79*, 74-80.
[25] Rahmani, M., Ghasemi, E., & Sasani, M. (2017). Application of response surface methodology for air assisted-dispersive liquid-liquid microextraction of deoxynivalenol in rice samples prior to HPLC-DAD analysis and comparison with solid phase extraction cleanup. *Talanta*, *165*, 27-32.
[26] Saad, M., Tahir, H., Khan, J., Hameed, U., & Saud, A. (2017). Synthesis of polyaniline nanoparticles and their application for the removal of Crystal Violet dye by ultrasonicated adsorption process based on Response Surface Methodology. *Ultrasonics sonochemistry*, *34*, 600-608.
[27] Chen, S., Zeng, Z., Hu, N., Bai, B., Wang, H., & Suo, Y. (2018). Simultaneous optimization of the ultrasound-assisted extraction for phenolic compounds content and antioxidant activity of Lycium ruthenicum Murr. fruit using response surface methodology. *Food chemistry*, *242*, 1-8.
[28] Dastkhoon, M., Ghaedi, M., Asfaram, A., Goudarzi, A., Mohammadi, S. M., & Wang, S. (2017). Improved adsorption performance of nanostructured composite by ultrasonic wave: Optimization through response surface methodology, isotherm and kinetic studies. *Ultrasonics sonochemistry*, *37*, 94-105.
[29] Ling, Z., Cao, J., Zhang, W., Zhang, Z., Fang, X., & Gao, X. (2018). Compact liquid cooling strategy with phase change materials for Li-ion batteries optimized using response surface methodology. *Applied Energy*, *228*, 777-788.
[30] Dayan, C. B., Afghah, F., Okan, B. S., Yıldız, M., Menceloglu, Y., Culha, M., & Koc, B. (2018). Modeling 3D melt electrospinning writing by response surface methodology. *Materials & Design*, *148*, 87-95.
[31] Davoudpour, Y., Hossain, S., Khalil, H. A., Haafiz, M. M., Ishak, Z. M., Hassan, A., & Sarker, Z. I. (2015). Optimization of high pressure homogenization parameters for the isolation of cellulosic nanofibers using response surface methodology. *Industrial Crops and Products*, *74*, 381-387.
[32] Khanlou, H. M., Ang, B. C., Talebian, S., Barzani, M. M., Silakhori, M., & Fauzi, H. (2015). Multi-response analysis in the processing of poly (methyl methacrylate) nano-fibres membrane by electrospinning based on response surface methodology: fibre diameter and bead formation. *Measurement*, *65*, 193-206.
[33] Gu, S., Ren, J., & Vancso, G. (2005). Process optimization and empirical modeling for electrospun polyacrylonitrile (PAN) nanofiber precursor of carbon nanofibers. *European polymer journal*, *41*, 2559-2568.
[34] Mellado, P., McIlwee, H. A., Badrossamay, M. R., Goss, J. A., Mahadevan, L., & Kit Parker, K. (2011). A simple model for nanofiber formation by rotary jet-spinning. *Applied Physics Letters*, *99*, 203107.
[35] Hong, X., Harker, A., & Edirisinghe, M. (2018). Process Modeling for the Fiber Diameter of Polymer, Spun by Pressure-Coupled Infusion Gyration. *ACS Omega*, *3*, 5470-5479.

[36] Zhang, X., & Lu, Y. (2014). Centrifugal Spinning: An Allternative Approach to Fabricate Nanofibers at High Speed and Low Cost. *Polymer Reviews*, *54*, 677-701.
[37] Mahalingam, S., & Edirisinghe, M. (2013). Forming of polymer nanofibers by a pressurised gyration process. *Macromolecular rapid communications*, *34*, 1134-1139.
[38] Casper, C. L., Stephens, J. S., Tassi, N. G., Chase, D. B., & Rabolt, J. F. (2004). Controlling Surface Morphology of Electrospun Polystyrene Fibers: Effect of Humidity and Molecular Weight in the Electrospinning Process. *Macromolecules*, *37*, 573-578.
[39] Barnes, W. J., & Price, F. P. (1961). Intrinsic and bulk viscosities of some polyethylene oxide polymers. *Journal of Polymer Science*, *50*, S25-S26.
[40] De Schoenmaker, B., Van Der Schueren, L., Ceylan, Ö., & De Clerck, K. (2012). Electrospun polyamide 4.6 nanofibrous nonwovens: parameter study and characterization. *Journal of Nanomaterials*, *2012*, 860654.
[41] Faridi-Majidi, R., Ziyadi, H., Naderi, N., & Amani, A. (2012). Use of artificial neural networks to determine parameters controlling the nanofibers diameter in electrospinning of nylon-6, 6. *Journal of Applied Polymer Science*, *124*, 1589-1597.
[42] Adabi, M., Saber, R., Faridi-Majidi, R., & Faridbod, F. (2015). Performance of electrodes synthesized with polyacrylonitrile-based carbon nanofibers for application in electrochemical sensors and biosensors. *Materials Science and Engineering: C*, *48*, 673-678.
[43] Forsgren, A., Gill, P. E., & Wright, M. H. (2002). Interior Methods for Nonlinear Optimization. *SIAM review*, *44*, 525-597.
[44] Gupta, P., Elkins, C., Long, T. E., & Wilkes, G. L. (2005). Electrospinning of linear homopolymers of poly (methyl methacrylate): exploring relationships between fiber formation, viscosity, molecular weight and concentration in a good solvent. *Polymer*, *46*, 4799-4810.
[45] Macossay, J., Marruffo, A., Rincon, R., Eubanks, T., & Kuang, A. (2007). Effect of needle diameter on nanofiber diameter and thermal properties of electrospun poly (methyl methacrylate). *Polymers for Advanced Technologies*, *18*, 180-183.